Hindawi
Journal of Applied Mathematics
Volume 2022, Article ID 8131528, 13 pages
https://doi.org/10.1155/2022/8131528

Review Article

Hydromagnetic Non-Newtonian Fluid Flow in a Convergent Conduit

Njue Caroline Wawira, Mathew Kinyanjui, and Kang'ethe Giterere

Department of Pure and Applied Mathematics, Jomo Kenyatta University of Agriculture and Technology, Juja, 62000-00200 Nairobi, Kenya

Correspondence should be addressed to Njue Caroline Wawira; wawira.caroline2021@students.jkuat.ac.ke

Received 30 September 2022; Revised 23 November 2022; Accepted 24 November 2022; Published 17 December 2022

Academic Editor: Oluwole D. Makinde

In the present study, a hydromagnetic non-Newtonian (dilatant) fluid flow in a convergent conduit, in the presence of a variable transverse magnetic field, has been investigated. The governing nonlinear partial differential equations are reduced to system of ordinary differential equations. These equations are solved numerically by the collocation method and implemented in MATLAB. The study determines the flow profiles and the impact of the flow parameters on the flow variables. Joule heating, variable viscosity, viscous dissipation, skin friction, the rate of heat transfer, and the induced magnetic field are taken into account. The obtained results are presented graphically and the impact of varying flow parameters on the skin friction coefficient and the Nusselt number is presented in tabular form. These results indicate that an increase in the Reynolds number, Eckert's number, and the Joule heating parameter increases the fluid's velocity, while an increase in the Hartmann number and the unsteadiness parameter decreases the convective heat transfer and the fluid's velocity. Further, the skin friction coefficient decreases with increase in the Reynolds number, the Hartmann number, and the Joule heating parameter. Therefore, a less viscous fluid is appropriate to facilitate the fluid's motion, but the presence of high magnetic field reduces the fluid's motion.

1. Introduction

The study of fluid flow through convergent (or divergent) conduits was pioneered by [1, 2], hence the name Jeffery-Hamel flow. This area has received numerous attention considering its broad application in industrial and biomechanical engineering. Some of the remarkable applications include the flow of liquid metals in the cooling systems of nuclear reactors, extrusion of molten polymers through converging dies, inlet/outlet fluid flow in dams, the development of stenosis in the arteries which affect the blood flow, and fluid flow in the convergent conduit leading to the Pelton wheel turbine.

In the Pelton turbines, the impulse of the fluid flowing through the convergent conduit is responsible for rotation of the Pelton wheel. The turbine is coupled with the electric generator for production of electricity. Therefore, it is important to maintain the fluid velocity high and constant to avoid frequency variation in the generator which would lead to short circuiting. The viscous flow behaviour of a fluid flowing through various conduit is either considered constant (Newtonian) or variable (non-Newtonian). However, the water flowing through the convergent conduit is often saturated with salt or sand particle; hence, it is non-Newtonian in nature and exhibits shear-thickening property (dilatant fluid).

According to the study [3], non-Newtonian fluids are divided into three categories, i.e., differential, integral, and rate fluid flows. The differential fluid flows exhibit the normal stress, shear-thinning, and shear-thickening properties.

On the other hand, the rate fluid flows explain the impact of retardation and relaxation times.

In the study [4], a steady mixed convection flow of a non-Newtonian fluid containing gyrotatic microorganism along a vertical plate embedded in a saturated non-Darcy porous medium is considered. The power law model was used to describe the nature of the non-Newtonian fluid. The governing ordinary differential equations are solved numerically by implementation on MATLAB bvp4c solvers. It is noted that the mixed convection parameter shows a high impact on the Nusselt number, the Sherwood number, and motile microorganism density profiles, but these parameters decrease mostly for pseudoplastic fluid.

[5] carried out a study on a two-dimensional, incompressible, steady, and non-Newtonian (Casson) flowing fluid over semi-infinite vertical plates taking into account the chemical reaction. The shear-thinning fluid (Casson fluid) exhibits an infinite viscosity at low shear rate. The model equations obtained are solved numerically by utilizing the Runge-Kutta-Fehlberg method with shooting technique. The results reveal that an increase in the activation energy increases the fluid velocity and heat transport in the Casson fluid system due to exothermic heat reaction.

Nagler [6] examined an unsteady fluid flow through a convergent conduit neglecting the body forces but considering the flowing fluid as non-Newtonian and accounting for the wall friction. In this study, the partial differential equations governing the flow were solved numerically by the collocation method. The nonlinear viscosity was based on the tangential coordinate function due to the radial geometry shape. He discovered that the Newtonian-normalized velocity reduces gradually with the tangential direction progress. The results showed that an increase in the friction coefficient led to a decrease in velocity values, but an increase in the Reynolds number increased the velocity profiles.

[7] investigated a two-dimensional, unsteady, incompressible fluid flow through convergent conduits. The study was applied in geothermal pipes where the fluid is in the gaseous and liquid states. The nonlinear partial differential equations were solved numerically using the collocation method. The results showed that an increase in the Prandtl number led to an increase in temperature at constant thermal conductivity. Similarly, an increase in the Eckert number increased the radial temperature resulting in an increased temperature gradient. Further, the results showed that the inclining of the convergent geothermal pipes would aid the control of deposition and control of heat in the convergent conduits.

[8] studied an unsteady two-dimensional Jeffery-Hamel flow of an incompressible non-Newtonian fluid flowing through a divergent conduit under a constant transverse magnetic field. The governing equations were solved numerically by the collocation technique and implemented in MATLAB. It was concluded that the fluid velocity and temperature increased with increasing values of the Reynolds number and the Hartmann number. Further, the skin friction coefficient increased with increasing values of the unsteadiness parameter.

[9] studied the hydromagnetic flow of a nanofluid through a convergent/divergent conduit with porous media using the Homotopy perturbation method to obtain a solution for the governing Naiver-Stokes equations. The results showed that an increase in the conduit's angle along the flow reduced the fluid flow. Consequently, the temperature is reduced with an increase in the Darcy number

Recently, [10] analysed the Cu-water nanofluid flow in a convergent-divergent channel where heat transfer and velocity profiles were examined taking into account the entropy generation. The nondimensional ordinary differential equations obtained were computed by the Hermite-Pade approximation (HPA) method to solve the power series. The results remarkably imply that entropy generation increased at the wall bringing a significant effect on the heat transfer and velocity profiles. Also, [11] investigated the bioconvective MHD Blasius and Sakiadis flow with the Cattaneo-Christov heat flux model and chemical reaction. The magnetic field in the study is considered constant. The partial differential equations governing the flow are transformed into ordinary differential equations and solved by the Galerkin numerical technique. In the study, the impact of the flow parameter on the velocity, temperature, and concentration is examined. It is observed that the increased magnetic field reduced the velocity in both the Sakiadis and Blasius flows, and concentration decreases with increase in the Lewis number and the bioconvective Peclet number.

However, in accordance with Faraday's law of induction [12], the mutual interaction of the magnetic field and the relative motion of the electrically conducting fluid, e.g., plasma, liquid metals, and salt solution, yield an electromotive force that alters the flow profiles. Induced current as per Ampere's law [13] induces magnetic field; hence, the total magnetic field is the imposed plus the induced magnetic field.

Further, in real-life problems, the passage of current through an electrically conducting fluid produces thermal energy (Joule heating), while a viscous fluid offers resistance to the motion of the fluid's layer over the adjacent layer of the fluid yielding thermal energy (viscous dissipation).

Therefore, in light of the prior studies on flow through convergent conduits, the Joule heating, viscous dissipation, and variable magnetic field have been neglected. Similarly, the rate of heat transfer and skin friction between the fluid and the conduit's wall has not been considered. Thus, the present study is motivated to provide a comprehensive insight into a hydromagnetic, unsteady, non-Newtonian (dilatant) fluid flowing through a convergent conduit in the presence of variable magnetic field. In the study, viscous dissipation, the Joule heating, skin friction, and the rate of heat transfer are taken into account.

The present work motivation entails the following novel aspects: first, the mathematical formulation of an unsteady, incompressible, non-Newtonian fluid flow through a convergent conduit taking into account the viscous dissipation, the Joule heating, skin friction, and heat transfer rate. The

nature of the non-Newtonian fluid is described by the power law model. Second, the governing PDEs are transformed into ODEs followed by reduction of the higher-order differential equations to first-order ODEs. The first-order ODEs are then solved numerically using the collocation method and its implementation in MATLAB. Finally, the flow profiles are determined, and the impact of the flow parameter on the flow profiles is examined and presented using graphs and a data table.

2. Problem Formulation

The present study considers an unsteady non-Newtonian hydromagnetic fluid flow through a convergent conduit in presence of a variable magnetic field where viscous dissipation, the Joule heating, skin friction, and the rate of heat transfer are taken into account. The non-Newtonian fluid considered is a shear-thickening fluid (dilatant fluid). The magnetic field is applied perpendicular to the direction of flow as shown in Figure 1. The fluid flow is restricted in the laminar domain, assumed to be in the radial direction, i.e., $V = (U_r, 0, 0)$, and no chemical reactions take place in the fluid. Further, the effect of pressure on the fluid's density is considered negligible, and the force due to induced electric field ρE is negligible compared to the Lorentz force $F = J \times B$ due to the magnetic field. A cylindrical coordinate system is chosen due to the nature of the conduit where the origin lies at the centre of the conduit, the r direction is measured from the wedge axis, θ from a convenient meridian plane, and z along the length of the conduit. The flow field is unbounded (infinite) in the z direction; thus, the partial derivatives with respect to z vanishes.

3. The Governing Equations

According to studies done by [7–9, 14] among other researchers, the fundamental equations governing the flow problem in cylindrical coordinate system can be expressed as

$$\frac{\partial (rU_r)}{\partial r} = 0, \tag{1}$$

$$\rho\left(\frac{\partial U_r}{\partial t} + U_r\frac{\partial U_r}{\partial r} + \frac{U_\theta}{r}\frac{\partial U_r}{\partial \theta} + U_z\frac{\partial U_r}{\partial z} - \frac{U_\theta^2}{r}\right) = -\frac{\partial P}{\partial r} + \left(\frac{1}{r}\frac{\partial (r\tau_{rr})}{\partial r} + \frac{1}{r}\frac{\partial \tau_{r\theta}}{\partial \theta} + \frac{\partial \tau_{rz}}{\partial z} - \frac{\tau_{\theta\theta}}{r}\right) + \rho F_r, \tag{2}$$

$$\rho\left(\frac{\partial U_\theta}{\partial t} + U_r\frac{\partial U_\theta}{\partial r} + \frac{U_\theta}{r}\frac{\partial U_\theta}{\partial \theta} + U_z\frac{\partial U_\theta}{\partial z} + \frac{U_\theta U_r}{r}\right) = -\frac{1}{r}\frac{\partial P}{\partial \theta} + \left(\frac{1}{r^2}\frac{\partial \left(r^2\tau_{\theta r}\right)}{\partial r} + \frac{1}{r}\frac{\partial \tau_{\theta\theta}}{\partial \theta} + \frac{\partial \tau_{\theta z}}{\partial z}\right) + \rho F_\theta, \tag{3}$$

$$\rho C_p\left(\frac{\partial T}{\partial t} + u_r\frac{\partial T}{\partial r} + \frac{u_\theta}{r}\frac{\partial T}{\partial \theta} + u_z\frac{\partial T}{\partial z}\right) = k\left[\frac{1}{r}\frac{\partial}{\partial r}\left(r\frac{\partial T}{\partial r}\right) + \frac{1}{r^2}\frac{\partial^2 T}{\partial \theta^2} + \frac{\partial^2 T}{\partial z^2}\right] + \phi + \frac{j^2}{\sigma}, \tag{4}$$

$$\frac{\partial H_r}{\partial t} = \frac{1}{\eta}\left[\frac{\partial^2 H_r}{\partial r^2} + \frac{1}{r}\frac{\partial H_r}{\partial r} + \frac{1}{r^2}\frac{\partial^2 H_r}{\partial \theta^2} + \frac{\partial^2 H_r}{\partial z^2}\right] - \mu_e\left[u_r\frac{\partial H_r}{\partial r} + \frac{u_r}{r}\frac{\partial H_r}{\partial \theta} - \frac{u_\theta H_\theta}{r} + U_z\frac{\partial H_r}{\partial z}\right], \tag{5}$$

where equation (1) is the continuity equation, equations (2) and (3) are the momentum equation in r and θ directions, equation (4) is the energy equation, and equation (5) is the magnetic induction equations in r direction.

From the shear stress matrix presented in [15] and considering the assumptions that the flow is incompressible, purely radial, and two-dimensional, the shear matrix is reduced to

$$\begin{pmatrix} \tau_{rr} & \tau_{r\theta} & \tau_{rz} \\ \tau_{\theta r} & \tau_{\theta\theta} & \tau_{\theta z} \\ \tau_{zr} & \tau_{z\theta} & \tau_{zz} \end{pmatrix} = \begin{pmatrix} 2\mu\dfrac{\partial U_r}{\partial r} & \dfrac{\mu}{r}\dfrac{\partial U_r}{\partial \theta} & 0 \\ \dfrac{\mu}{r}\dfrac{\partial U_r}{\partial \theta} & 2\mu\left(\dfrac{U_r}{r}\right) & 0 \\ 0 & 0 & 0 \end{pmatrix}. \tag{6}$$

Therefore, the respective shear stress components in matrix (6) are substituted into the momentum equations. However, the fluid exhibits a nonlinear viscosity which is a function of the tangential direction. Thus, the power law model, $\tau = \mu_o(du_r/d\theta)^n$, is used to describe the nature of the non-Newtonian fluid. According to [4], μ_o is the consistency index, $du_r/d\theta$ is the velocity gradient, and n is the power law index. When $n < 1$, $n = 1$, and $n > 1$, the fluid is referred to as pseudoplastic, Newtonian, and dilatant fluids, respectively. The present study is devoted to a dilatant fluid which is non-Newtonian in nature and exhibits shear-thickening behaviour, e.g., quicksand. From the power law model,

$$\tau = \mu_o\left(\frac{du_r}{d\theta}\right)^n \Longrightarrow \tau = \mu_o\left(\frac{du_r}{d\theta}\right)^{n-1}\cdot\left(\frac{du_r}{d\theta}\right). \tag{7}$$

Hence, the viscosity is expressed as

$$\mu = \mu_o g^{n-1}, \tag{8}$$

where $g = g(\theta) = du_r/d\theta$ and the value assigned to n is greater than one to exhibit the dilatant fluid property.

3.1. Ohm's Law. The Ohm law establishes the fluid's ability to transport electric charges under magnetic field. The fluid's motion induces an electric current which exerts a force on the charged particles giving rise to induced current density J.

$$J = \sigma(E + V \times B). \tag{9}$$

The force is the Lorentz force given by $J \times B$. Therefore, the total electromagnetic force as per [13] is given as

$$F = \frac{1}{\rho}(\rho_e E + J \times B). \tag{10}$$

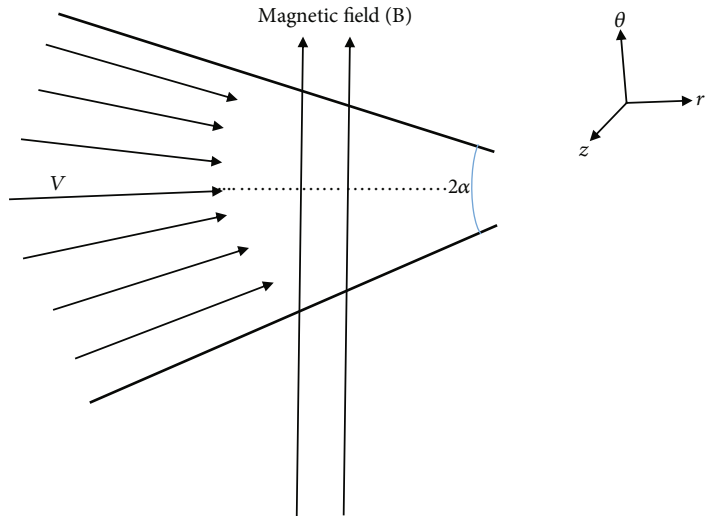

Figure 1: Flow geometry for a laminar flow in the radial direction.

The total magnetic field is given by adding the applied and induced magnetic field, i.e.,

$$(H^* + H) = (H_r^* + H_r)r + (H_\theta^* + H_\theta) + (H_z^* + H_z)z. \quad (11)$$

However, taking into account, the flow is two-dimensional, the applied magnetic field is in the θ direction and the direction of the induced magnetic field, and the total magnetic field is given as $(H^* + H) = H_r r + H_\theta^*$;

Thus,

$$J = \sigma(u_r \times B) = \sigma \begin{vmatrix} r & \theta & z \\ u_r & 0 & 0 \\ \mu_e H_r & \mu_e H_\theta^* & 0 \end{vmatrix} = \sigma \mu_e u_r H_\theta^* z, \quad (12)$$

and the body force becomes

$$F = \frac{1}{\rho}(J \times B) = \frac{1}{\rho} \begin{vmatrix} r & \theta & z \\ 0 & 0 & \sigma \mu_e u_r H_\theta^* \\ \mu_e H_r & \mu_e H_\theta^* & 0 \end{vmatrix} = -\frac{\sigma}{\rho} u_r \mu_e^2 H_\theta^{*2} r + \frac{\sigma}{\rho} u_r \mu_e^2 H_\theta^* H_r \theta. \quad (13)$$

The specific equations governing the flow are the momentum, energy, and magnetic induction equations. These equations are presented below, taking into account the Joule heating and viscous dissipation in the energy equation and the Lorentz force in the momentum equation.

3.1.1. Momentum Equation.

$$\frac{\partial^2 U_r}{\partial \theta \partial t} = \frac{1}{\rho r^2}\frac{\partial U_r}{\partial \theta}\frac{\partial^2 \mu}{\partial \theta^2} + \frac{\partial \mu}{\partial \theta}\left(\frac{2}{\rho r^2}\frac{\partial^2 U_r}{\partial \theta^2} + \frac{2U_r}{\rho r^2} - \frac{2}{\rho r^2}\frac{\partial U_r}{\partial r}\right) + \frac{\mu}{\rho}\left(\frac{1}{r^2}\frac{\partial^3 U_r}{\partial \theta^3} - \frac{2}{r}\frac{\partial^2 U_r}{\partial r \partial \theta} + \frac{2}{r^2}\frac{\partial U_r}{\partial \theta}\right) - U_r \frac{\partial^2 U_r}{\partial \theta \partial r} - \frac{\partial U_r}{\partial r}\frac{\partial U_r}{\partial \theta} - \frac{\sigma \mu_e^2 H_\theta^{*2}}{\rho}\frac{\partial U_r}{\partial \theta} - \frac{\sigma \mu_e^2 U_r H_\theta^* H_r}{\rho} - \frac{\sigma r \mu_e^2 H_\theta^* H_r}{\rho}\frac{\partial U_r}{\partial r} - \frac{\sigma r U_r \mu_e^2 H_\theta^*}{\rho}\frac{\partial H_r}{\partial r}. \quad (14)$$

According to [15], viscous dissipation is given by the expression

$$\phi = 2\mu\left[\left(\frac{\partial u_r}{\partial r}\right)^2 + \left(\frac{1}{r}\frac{\partial u\theta}{\partial \theta} + \frac{u_r}{r}\right)^2 + \left(\frac{\partial u_z}{\partial z}\right)^2\right] + \mu\left[\left(\frac{1}{r}\frac{\partial u_r}{\partial \theta} + \frac{\partial u_\theta}{\partial r} - \frac{u_\theta}{r}\right)^2 + \left(\frac{\partial u_\theta}{\partial z} + \frac{1}{r}\frac{\partial u_z}{\partial \theta}\right)^2 + \left(\frac{\partial u_z}{\partial \theta}\right)^2 + \left(\frac{\partial u_z}{\partial r} + \frac{\partial u_r}{\partial z}\right)^2\right]. \quad (15)$$

However, since the fluid flow is considered purely radial, two-dimensional, and non-Newtonian in nature, then the viscous dissipation is given as

$$\phi = 2\mu_o g^{n-1}\left[\left(\frac{\partial u_r}{\partial r}\right)^2 + \left(\frac{u_r}{r}\right)^2\right] + \mu_o g^{n-1}\left[\left(\frac{1}{r}\frac{\partial u_r}{\partial \theta}\right)^2\right]. \quad (16)$$

3.1.2. Energy Equation.

$$\begin{aligned}\frac{\partial T}{\partial t} &= \frac{k}{\rho C_p}\left[\frac{1}{r}\frac{\partial T}{\partial r} + \frac{\partial^2 T}{\partial r^2} + \frac{1}{r^2}\frac{\partial^2 T}{\partial \theta^2}\right] \\ &+ \frac{2\mu_o g^{n-1}}{\rho C_p}\left[\left(\frac{\partial u_r}{\partial r}\right)^2 + \left(\frac{u_r}{r}\right)^2\right] \\ &+ \frac{2\mu_o g^{n-1}}{\rho C_p}\left[\left(\frac{1}{r}\frac{\partial u_r}{\partial \theta}\right)^2\right] \\ &- u_r\frac{\partial T}{\partial r} + \frac{\sigma\mu_e^2 u_r^2 H_\theta^{*2}}{\rho C_p}.\end{aligned} \tag{17}$$

3.1.3. Magnetic Induction Equation.

$$\frac{\partial H_r}{\partial t} = \frac{1}{\eta}\left[\frac{\partial^2 H_r}{\partial r^2} + \frac{1}{r}\frac{\partial H_r}{\partial r} + \frac{1}{r^2}\frac{\partial^2 H_r}{\partial \theta^2}\right] - \mu_e u_r\frac{\partial H_r}{\partial r}. \tag{18}$$

The system of partial differential equations (14), (17), and (18) is conveniently transformed into ordinary differential equations which enables the nondimensionalization process hence ensuring that the obtained results are applicable to similar geometry configurations under the same conditions.

The following similarity transformations for velocity, viscosity, temperature, and magnetic field are used as presented in [14];

$$\begin{aligned}U_r(\theta, t) &= -\frac{Q}{r}\frac{1}{\delta^{m+1}}F(\theta), \\ \mu &= \mu_o\theta^{c(n-1)}(\theta), \\ \frac{\omega(\theta)}{\delta^{m+1}} &= \frac{T - T_w}{T_\infty - T_w}, \\ H_r(\theta, t) &= -\frac{Q}{r}\frac{1}{\delta^{m+1}}\gamma(\theta).\end{aligned} \tag{19}$$

Therefore, the final set of the dimensionless ordinary differential equations governing the flow problem is as follows:

$$\begin{aligned}&c(n-1)\theta^{c(n-1)-2}[c(n-1)-1]F' + c(n-1)\theta^{c(n-1)-1}\left[2F'' + 4F\right] \\ &+ \theta^{c(n-1)}\left[F''' + 4F'\right] - 2R_e\frac{r}{\delta^{m+1}}FF' - \mathrm{Ha}^2F' \\ &- R_m\frac{\mathrm{Ha}}{r\sqrt{\sigma\mu_o}}\frac{1}{\delta^{m+1}}\gamma F + (m+1)\frac{r^{m+1}}{\delta^{m+1}}\lambda F' = 0,\end{aligned} \tag{20}$$

$$(m+1)\frac{r^{m+1}}{\delta^{m+1}}\lambda\omega + \frac{1}{\mathrm{Pr}}\omega'' + \theta^{c(n-1)}\frac{\mathrm{Ec}}{\delta^{m+1}}\left[4F^2 + F'^2\right] + \frac{J}{\delta^{m+1}}F^2 = 0, \tag{21}$$

$$(m+1)\frac{r^{m+1}}{\delta^{2m+2}}\lambda\gamma + \frac{1}{\mathrm{Pr}_{(m)}}\frac{1}{\delta^{m+1}}\left[\gamma + \gamma''\right] - \mathrm{Re}\,\mu_e\frac{r}{\delta^{2m+2}}F\gamma = 0. \tag{22}$$

3.2. Dimensionless Parameters. The dimensionless parameters appearing in the above equations are defined as follows: the unsteadiness parameter $\lambda = ((\rho\delta^m)/(\mu_o r^{m-1}))(d\delta/dt)$ takes into account the time factor for an unsteady flow. The Prandtl number $\mathrm{Pr} = \mu_o/\rho\alpha$ where $\alpha = k/(\rho C_p)$ considers the relation between the thermal and momentum diffusivity. The Eckert number $\mathrm{Ec} = (Q^2/r^2)\,(1/(C_p(T_\infty - T_w)))$ gives the relation of the fluid's kinetic energy and the boundary layer enthalpy difference. The Joule heating parameter $J = (\sigma\mu_e^2 H_\theta^{*2}Q^2)/(\mu_o C_p(T_\infty - T_w))$ describes the physical phenomenon, where the passage of current through an electrically conducting fluid produces thermal energy. The Reynolds number $R_e = Q\rho/r\mu_o$ describes the flow behaviour as laminar or turbulent. The magnetic Prandtl number $\mathrm{P}\,\mathrm{r}_{(m)} = \mu_e\sigma\mu_o/\rho$ explains the momentum diffusivity to the magnetic diffusivity in the fluid. The magnetic Reynolds number $R_m = \mu_e\sigma(Q/r)$ estimates the effects of the induced magnetic field due to the motion of the conducting fluid to the magnetic diffusion. The Hartmann number $\mathrm{Ha} = B_o r(\sigma/\mu_o)^{1/2}$ gives the relation between electromagnetic forces to the viscous force due to the presence of the magnetic field.

3.3. Parameters of Practical Interest

3.3.1. Wedge Angle Parameters. According to [16], the wedge angle parameter is expressed as $\Omega = (2m/(m+1))\pi$. However, in the present study, the wedge angle is 2α, hence the relation $\Omega = 2\alpha = (2m/(m+1))\pi \Longrightarrow \alpha = (m/(m+1))\pi$.

The wedge angle parameter provides the relationship between the angle α and the arbitrary constant m.

The velocity, temperature, and magnetic induction profiles are evaluated by taking different values for the wedge angle parameter, considering the fact that the flow takes place in a convergent conduit, $\alpha = [0, 45^\circ]$ which is equivalent to [0,0.7854rad]. For instance,

$$\begin{aligned}&m = \frac{1}{3} = 0.3333.;\alpha = \frac{\pi}{4} = 45^\circ,\ m = \frac{1}{4} = 0.25\,;\ \alpha = \frac{\pi}{5} = 36^\circ, \\ &m = \frac{1}{5} = 0.2\,;\ \alpha = \frac{\pi}{6} = 30^\circ,\ m = \frac{1}{6} = 0.1667.;\alpha = \frac{\pi}{7} = 25.7^\circ.\end{aligned} \tag{23}$$

3.3.2. Skin Friction Coefficient. According to [17], skin friction coefficient is a significant dimensionless parameter in boundary layer flows which is obtained from the expression

$$C_f = \frac{2}{\sqrt{\mathrm{Re}\,(2-\varepsilon)}}F'(\theta), \tag{24}$$

where $\varepsilon = 2m/(m+1)$.

The skin friction coefficient provides information on the maximum possible friction force that exists between the fluid in motion and wall surface.

3.3.3. Nusselt Number. According to [17], the Nusselt number provides a significant relationship between the heat transfer due to convection and heat transfer due to

conduction. The Nusselt number is obtained from the expression

$$\mathrm{Nu} = -\sqrt{\frac{\mathrm{Re}}{2-\varepsilon}}\omega'(\theta). \tag{25}$$

Further, the Nusselt number is directly proportional to the negative temperature gradient.

3.4. Boundary Condition. The following boundary conditions were applied as presented in [8, 9, 14], where the no-slip condition on the conduit's wall was considered.

At the centreline, $U_r = U_\infty$, $(\partial U_r)/\partial\theta = 0$, $T = T_\infty$, and $\partial T/\partial\theta = 0$ at $\theta = 0$.

On the conduit's wall, $(\partial U_r)/\partial\theta = -\beta F(\theta)$ and $T = T_w$ at $\theta = \alpha$.

On applying the similarity transformation technique on the boundary condition yields

$$\begin{aligned}&\text{At the centreline, } \theta = 0\,;\, F(0) = 1,\, F'(0) = 0, \omega(0) = \delta^{m+1},\\ &\text{On the conduit's wall, } \theta = \alpha\; F'(\alpha) = -\beta F(\alpha), \omega(\alpha) = 0.\end{aligned} \tag{26}$$

3.5. Method of Solution. The differential equations governing the flow are essentially nonlinear. Considering the nature of the flow geometry and the nonlinearity of the governing equations, the finite methods are less accurate and difficult to employ since much computational is required. Therefore, the collocation method is more appropriate for solving a two-point boundary value problem (BVP).

According to [18], the bvp4c function is implemented in MATLAB to solve a large class of two-point BVPs of the form below using the collocation method.

$$y'(\theta) = f(\theta, y(\theta))\,;\theta \in [a, b], \tag{27}$$

subject to general nonlinear, two-point boundary conditions

$$g(y(a), y(b)) = 0. \tag{28}$$

Therefore, the higher-order ODEs (20)–(22) are reduced to first-order ODEs using the definitions in equation (29). These definitions are obtained from the basic idea of introduction of new variables, where each variable and its derivatives in the equations is assigned a new variable up to one less the highest derivative.

$$\begin{aligned}y_1 &= F,\\ y_2 &= F',\\ y_3 &= F'',\\ y_4 &= \omega,\\ y_5 &= \omega',\\ y_6 &= \gamma,\\ y_7 &= \gamma'.\end{aligned} \tag{29}$$

Substituting the respective definitions in equation (29) into equations (20)–(22), i.e., the momentum, energy, and magnetic induction equations, respectively, we obtain

$$\begin{aligned}&c(n-1)\theta^{c(n-1)-2}[c(n-1)-1]y_2 + c(n-1)\theta^{c(n-1)-1}[2y_3 + 4y_1]\\ &\quad + \theta^{c(n-1)}\left[y_3' + 4y_2\right] - 2R_e\frac{r}{\delta^{m+1}}y_1y_2 - \mathrm{Ha}^2y_2\\ &\quad - R_m\frac{\mathrm{Ha}}{r\sqrt{\sigma\mu_o}}\frac{1}{\delta^{m+1}}y_6y_1 + (m+1)\frac{r^{m+1}}{\delta^{m+1}}\lambda y_2 = 0,\\ &(m+1)\frac{r^{m+1}}{\delta^{m+1}}\lambda y_4 + \frac{1}{\mathrm{Pr}}y_5' + \theta^{c(n-1)}\frac{\mathrm{Ec}}{\delta^{m+1}}\left[4y_1^2 + y_2^2\right] + \frac{J}{\delta^{m+1}}y_1^2 = 0,\\ &(m+1)\frac{r^{m+1}}{\delta^{2m+2}}\lambda y_6 + \frac{1}{\mathrm{Pr}_{(m)}}\frac{1}{\delta^{m+1}}\left[y_6 + y_7'\right] - \mathrm{Re}\;\mu_e\frac{r}{\delta^{2m+m}}y_1y_6 = 0,\end{aligned} \tag{30}$$

where

$$\begin{aligned}&y_1' = F' = y_2,\\ &y_2' = F'' = y_3,\\ &y_3' = F'' = \frac{-c(n-1)\theta^{c(n-1)-2}[c(n-1)-1]y_2 - c(n-1)\theta^{c(n-1)-1}[2y_3 + 4y_1] + \left(2R_e\left(r/\delta^{m+1}\right)\right)y_1y_2 + \mathrm{Ha}^2y_2 + \left(R_m\left(\mathrm{Ha}/r\sqrt{\sigma\mu_o}\right)\right)\left(1/\delta^{m+1}\right)y_6y_1 - (m+1)\left(\left(r^{m+1}\right)/\left(\delta^{m+1}\right)\right)\lambda y_2}{\theta^{c(n-1)}}\\ &\qquad - 4y_2(A),\\ &y_4' = \omega' = y_5,\\ &y_5' = \omega'' = \mathrm{Pr}\left[-(m+1)\frac{r^{m+1}}{\delta^{m+1}}\lambda y_4 - \theta^{c(n-1)}\frac{\mathrm{Ec}}{\delta^{m+1}}\left[4y_1^2 + y_2^2\right] - \frac{J}{\delta^{m+1}}y_1^2\right](B), y_6' = \gamma' = y_7,\\ &y_7' = \gamma'' = \left[-(m+1)\frac{r^{m+1}}{\delta^{2m+2}}\lambda y_6 + \mathrm{Re}\;\mu_e\frac{r}{\delta^{2m+m}}y_1y_6\right]\mathrm{Pr}_{(m)}\delta^{m+1} - y_6\,(C).\end{aligned} \tag{31}$$

In matrix form,

$$y = \begin{pmatrix} y_1 \\ y_2 \\ y_3 \\ y_4 \\ y_5 \\ y_6 \\ y_7 \end{pmatrix} \quad f = y' = \begin{pmatrix} y_2 \\ y_3 \\ A \\ y_5 \\ B \\ y_7 \\ C \end{pmatrix}. \tag{32}$$

The bvp4c function mainly introduces a residual control-based adaptive mesh solver. The adaptive solver adjusts the mesh points in an iterative procedure hence gaining control over the grid resolution. This is advantageous in terms that it is easy to program, provides highly accurate solution, has a high convergence since the solution tends to the exact values on reduction of the stepsize $(h \longrightarrow 0)$, and utilizes low computational memory.

Further, reducing the order of the boundary conditions in equation (26) using the respective definitions in equation (29) gives

$$\begin{aligned} &\text{At the centreline, } \theta = 0\,; y_1(0) = 1, y_2(0) = 0, y_4(0) = \delta^{m+1}, \\ &\text{On the conduit}'\text{s wall, } \theta = \alpha\,; y_2(\alpha) = -\beta y_1(\alpha), y_4(\alpha) = 0. \end{aligned} \tag{33}$$

4. Results and Discussion

The results obtained are presented using graphs and a data table which is followed by a discussion. The velocity, temperature, and magnetic induction profiles are determined followed by the effect of varying flow parameters on the profiles.

From Figure 2, it is observed that velocity increases with decrease in the wedge angle. This implies that the velocity is high at the centreline and decreases towards the conduit's wall. This is due to the fact that the viscous forces at the wall are high which tend to resist the fluid's motion.

In Figure 3, it is observed that the fluid temperature decreases with increase in the wedge angle. This is because viscosity is inversely proportional to temperature in liquids. Thus, as the fluid viscosity increases the fluid's temperatures reduces. Further, this is justified by the reduced velocity towards the wall which leads to less conversion of the kinetic energy into thermal energy leading to the decrease in temperature.

From Figure 4, it is observed that magnetic induction increases with decrease in the wedge angle. This is because the fluid's velocity increases with decrease in the wedge angle. Therefore, at the centreline of the conduit, there is a high interaction between the applied magnetic field and the fluid velocity. This increases the induced electric current, which in turn increases the induced magnetic field.

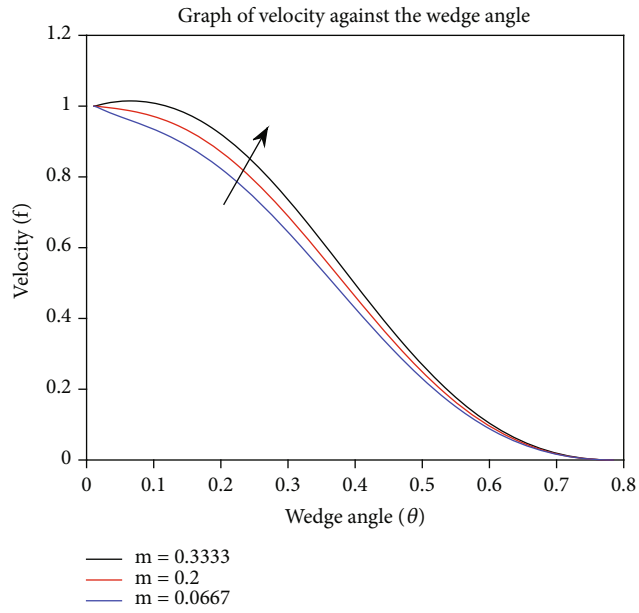

Figure 2: Velocity profiles.

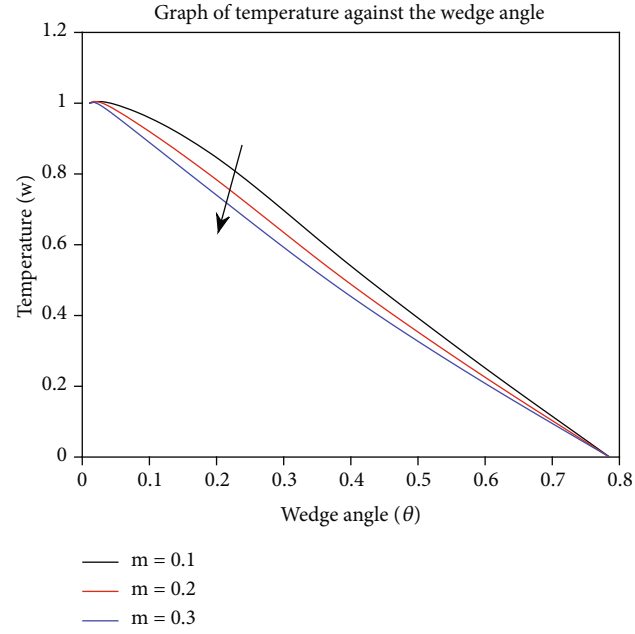

Figure 3: Temperature profiles.

From Figure 5, it is observed that an increase in the Reynolds number increases the fluid's velocity. An increase in the Reynolds number implies that the viscous forces are minimal and the inertia forces predominate. Therefore, there is minimal retardation of the fluid's motion since the boundary layer formed does not extend extremely into the flow region. This explains the increase in velocity with increase in the Reynolds number.

From Figure 6, it is observed that temperature increases with increase in the Reynolds number. An increase in the Reynolds number implies that the viscosity is minimal.

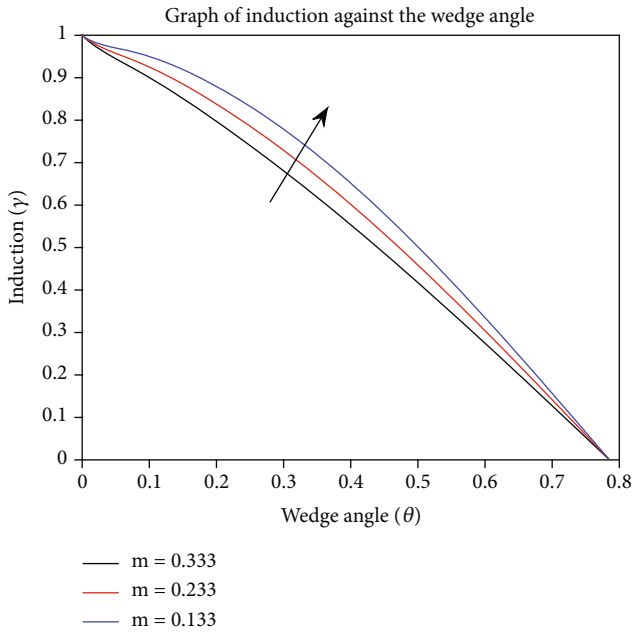

Figure 4: Magnetic induction profiles.

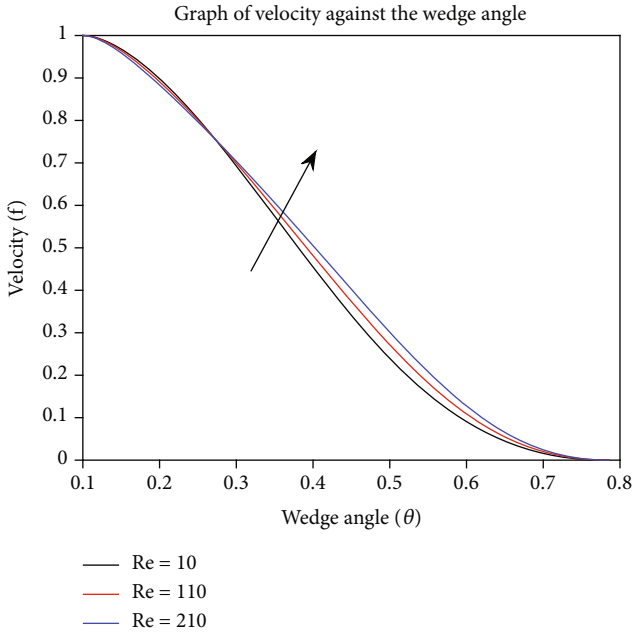

Figure 5: Effect of varying the Reynolds number on velocity.

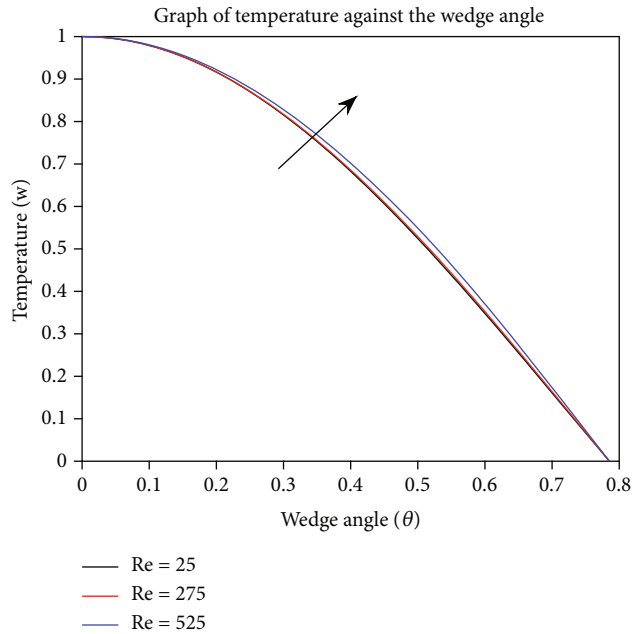

Figure 6: Effect of varying the Reynolds number on temperature.

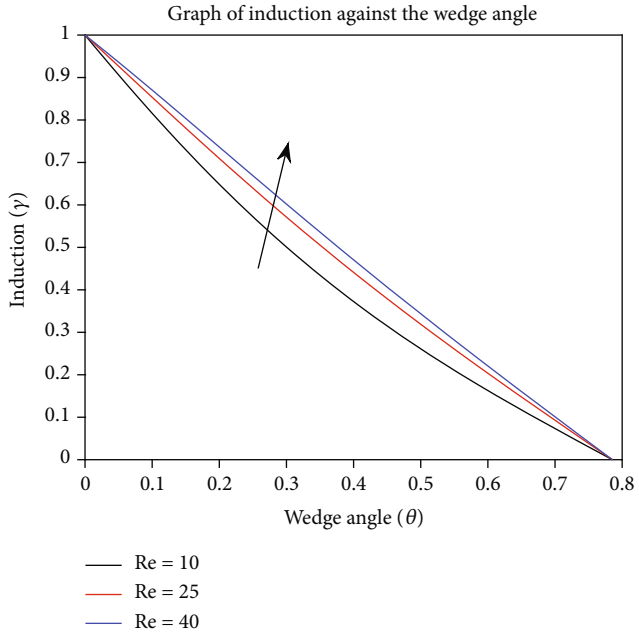

Figure 7: Effect of varying the Reynolds number on magnetic induction.

However, viscosity is inversely proportional to temperature in liquids. Therefore, the fluid temperature increases at minimal viscosity.

From Figure 7, it is observed that magnetic induction increases with the increase in the Reynolds number. An increase in the Reynolds number implies that the inertia forces dominate; hence, the fluid's motion is accelerated. Therefore, as per equation (12), an increase in the velocity leads to an increase in the induced current. However, as per Ampere's law [13], the induced electric current also produces induced magnetic field. Thus, the increase in the induced electric current increases the induced magnetic field.

From Figure 8, it is observed that an increase in the Hartmann number decreases the fluid's velocity. An increase in the Hartmann number implies that the electromagnetic force dominates; hence, the effect of viscous drag is minimal. Further, the present magnetic field interacts with the fluid velocity, yielding the Lorentz force that acts against the direction of flow. Thus, an increase in the Hartmann

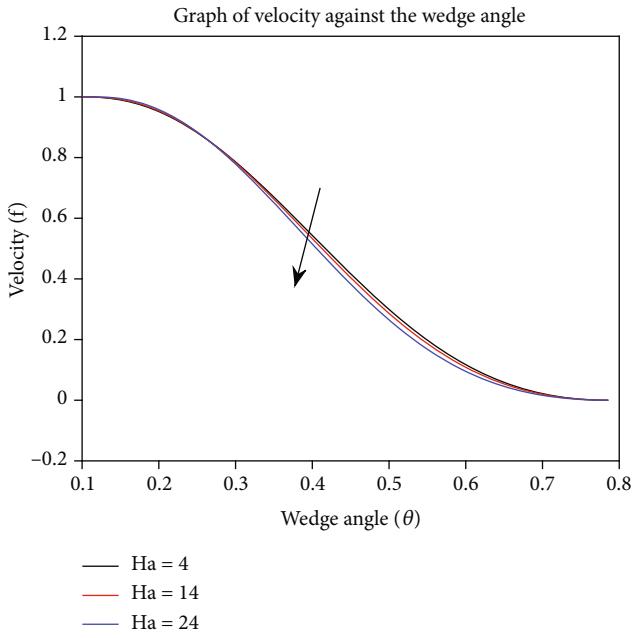

Figure 8: Effect of varying the Hartmann number on velocity.

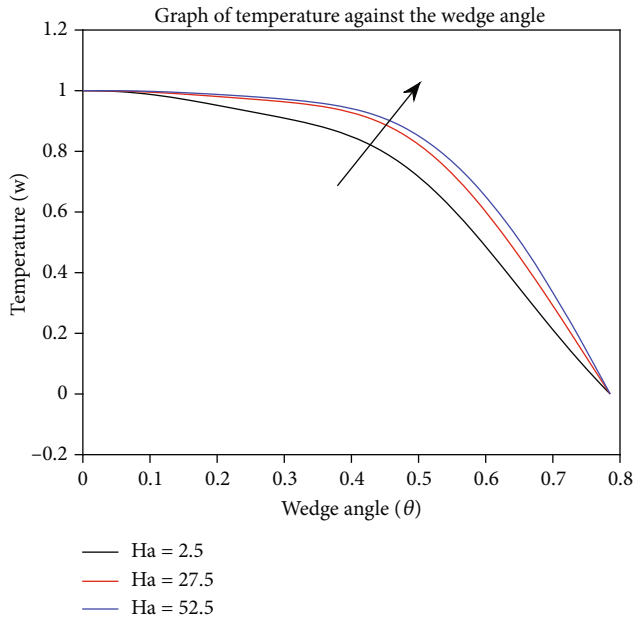

Figure 9: Effect of varying the Hartmann number on temperature.

number leads to an increase in the Lorentz force which in turn retards the fluid's motion.

From Figure 9, it is observed that increase in the Hartmann number increases the fluid's temperature. The presence of magnetic field yield the Lorentz force that acts against the fluid flow. This increases the resistance to the fluid motion which in turn increases the fluid's temperature. Further, an increase in the Hartmann number implies that the viscous forces decreases; hence, the temperature of the fluid increases, since viscosity and temperature are inversely proportional in liquids.

From Figure 10, it is observed that magnetic induction decreases with increase in the Hartmann number. An increase in the Hartmann number implies that viscous forces are minimal; hence, the Lorentz force predominates. However, the Lorentz force retards the fluid's motion hence decreasing the fluid's velocity. This leads to less interaction between the applied magnetic field and the fluid velocity. This implies that less electric current is induced in the electrically conducting fluid, which in turn decreases the induced magnetic field.

From Figure 11, the velocity increases with increase in the Joule heating parameter. An increase in the Joule heating parameter implies that the amount of heat energy emitted as electric current passing through the electrically conducting fluid increases. Therefore, an increase in the Joule heating parameter increases the fluid's temperature, which leads to a decrease in the fluid's viscosity. Thus, the fluid's velocity increases.

From Figure 12, it is observed that an increase in the Joule heating parameter increases fluid temperature. The increase in the Joule heating parameter implies that the amount of electric current passing through the electrically conducting fluid increases hence increasing the amount of heat energy released. This leads to an increase in the fluid's temperature due to heating of the fluid's particles.

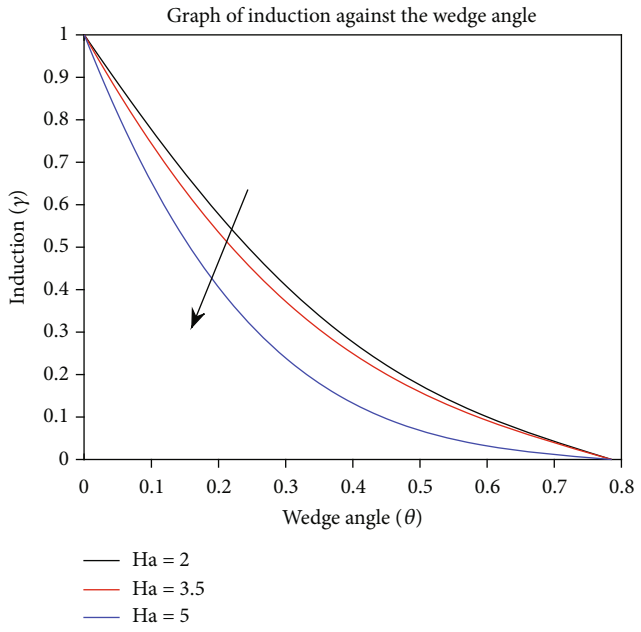

Figure 10: Effect of varying the Hartmann number on magnetic Induction.

From Figure 13, the magnetic induction increases with increase in the Joule heating parameter. According to Ampere's law, the induced electric current induces magnetic field. Therefore, an increase in the Joule heating parameter implies that the amount of electric current passing through the fluid increases. Hence, with the increase in the electric current in the flow, the induced magnetic field increases. Further, increasing the Joule heating parameter increases the fluid's velocity, which increases the interaction between

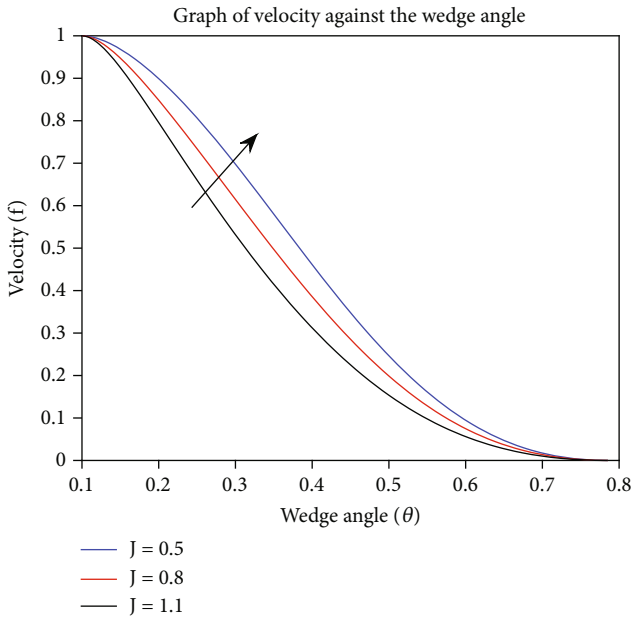

Figure 11: Effect of varying the Joule heating parameter on velocity.

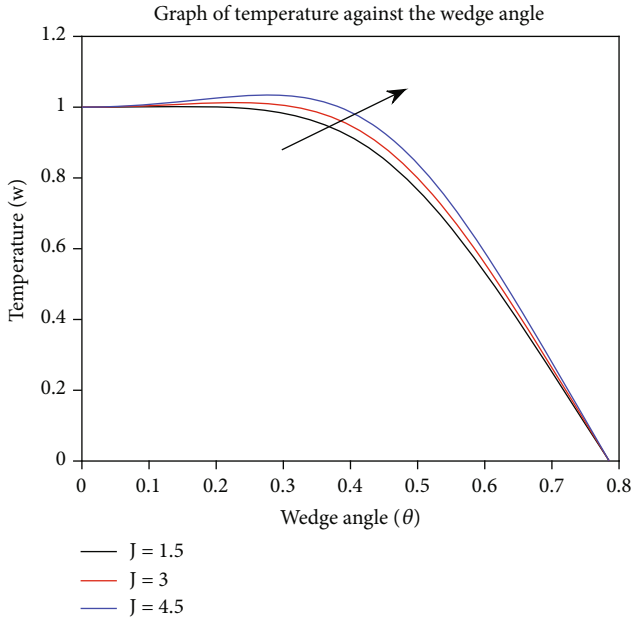

Figure 12: Effect of varying the Joule heating parameter on temperature.

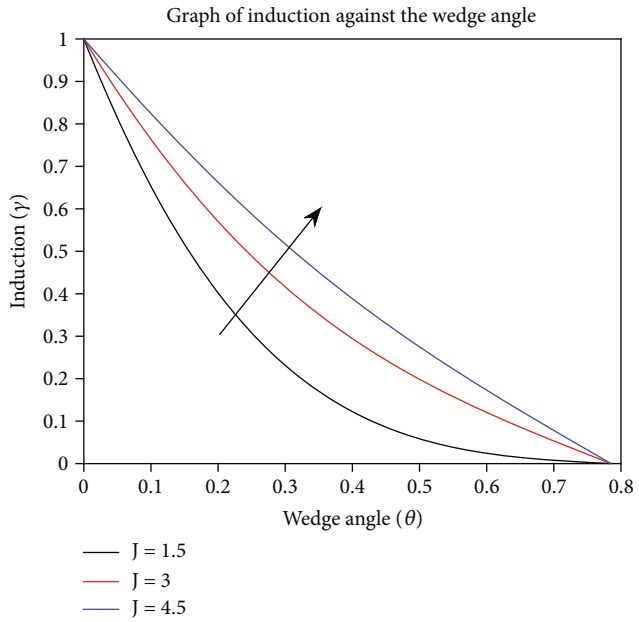

Figure 13: Effect of varying the Joule heating parameter on magnetic induction.

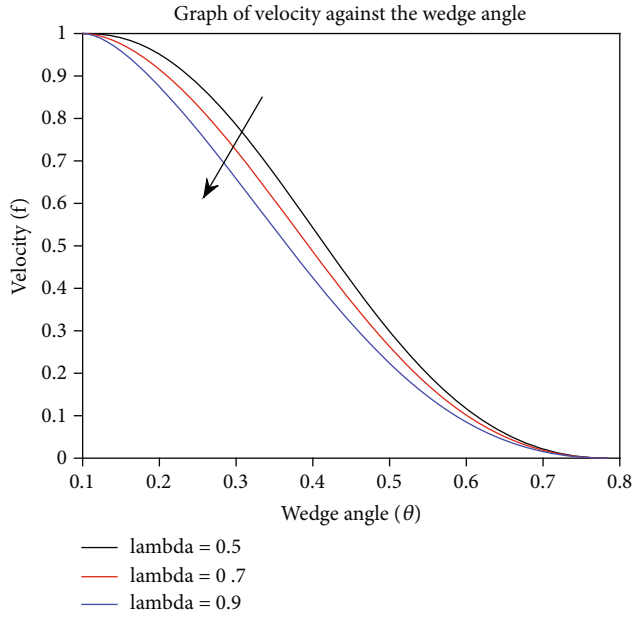

Figure 14: Effect of varying the unsteadiness parameter on velocity.

the applied magnetic field and velocity; hence, the induced magnetic field increases.

From Figure 14, it is observed that velocity decreases with increase in the unsteadiness parameter. The unsteadiness parameter caters for the time factor. In the present study, the unsteadiness parameter and time dependent length scale δ are directly proportional. However, from the equation $v = d/t$, velocity and time are inversely proportional. Therefore, an increase in unsteadiness parameter decreases the velocity. Further, an increase in the unsteadiness parameter implies that the boundary layer extends into the flow region which increases the viscous drag forces, hence reducing the fluid's velocity.

From Figure 15, it is observed that temperature increases with increase in the unsteadiness parameter. An increase in the unsteadiness parameter implies that the boundary layer tends towards the centreline of the conduit. This increases the fluid resistance to motion, due to the increase in viscous

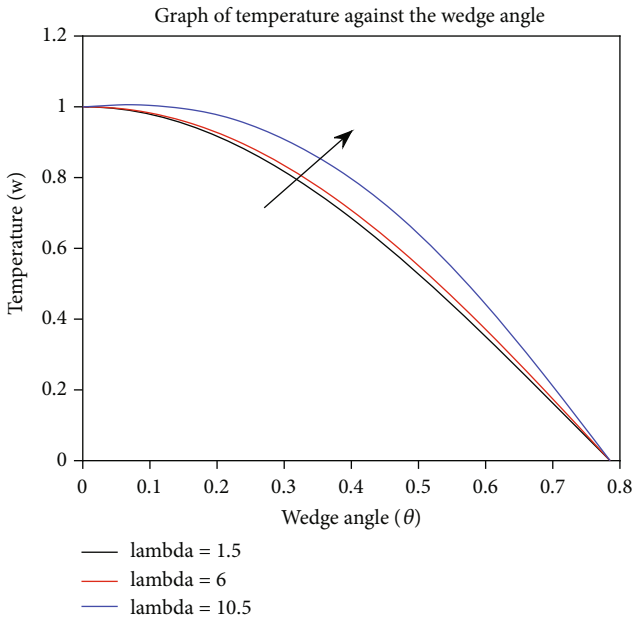

Figure 15: Effect of varying the unsteadiness parameter on temperature.

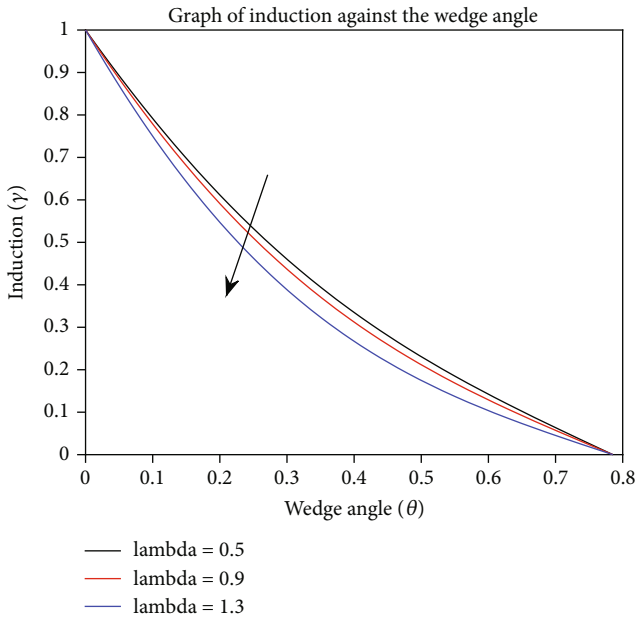

Figure 16: Effect of varying the unsteadiness parameter on magnetic induction.

forces. Hence, the resistance to motion between one layer over the adjacent layer produces thermal energy which increases the fluid's temperature.

From Figure 16, magnetic induction decreases with increase in the unsteadiness parameter. An increase in the unsteadiness parameter increases the viscous force due to the extension of the boundary layer into the flow region. This reduces the fluid's velocity, which consequently reduces the induced electric current. Thus, with less induced current, the induced magnetic field is minimal.

From Table 1, variation of various flow parameters on skin friction and the Nusselt number provided the following deductions. The skin friction coefficient provides information on the maximum friction force that exists between the fluid in motion and the conduit's wall. An increase in the Reynolds number decreased the skin friction coefficient. This is because an increase in the Reynolds number implies that the viscous forces are minimal; hence, the inertia force facilitates the fluid's motion thus minimizing the friction forces. Further, an increase in the Hartman number leads to a decrease in the skin friction coefficient. The Hartman number shows the relation between the drag due to magnetic induction and the viscous force. Therefore, the increase in Hartmann number implies that the viscous forces are minimal hence less formation and extension of the boundary layer into the flow region.

Similarly, an increase in the Joule heating parameter decreases the skin friction coefficient. An increase in the Joule heating parameter implies that the heat energy emitted increases hence an increase in temperature which minimizes the viscous and friction forces. However, an increase in unsteadiness parameter led to an increase in skin friction coefficient. The unsteadiness parameter caters for the time factor. Therefore, as time elapses, the boundary layer formed extends into the flow region hence retarding the fluid in motion due to increased viscosity and friction force.

Table 1: Skin friction coefficient and the Nusselt number values on variation of the flow parameters, i.e., the Reynolds number, the Hartmann number, the Joule heating parameter, and the unsteadiness parameter.

Skin friction coefficient	Nusselt number	Re	Ha	J	λ
0.0710	0.0062	**3**	4	6	1.5
0.0587	0.0163	**7**	4	6	1.5
0.0515	0.0208	**11**	4	6	1.5
0.0466	0.0316	**15**	4	6	1.5
0.1559	1.0519	25	**10**	6	1.5
0.1308	0.1251	25	**20**	6	1.5
0.0970	0.0207	25	**30**	6	1.5
0.0569	0.0118	25	**40**	6	1.5
-0.1559	0.0040	25	4	**4**	1.5
-0.6380	0.0240	25	4	**7**	1.5
-0.6025	0.0475	25	4	**10**	1.5
-0.9751	0.0623	25	4	**13**	1.5
0.1559	0.0189	25	4	6	**0.5**
0.5261	0.0156	25	4	6	**1**
1.2960	0.0027	25	4	6	**1.5**
7.4444	0.0016	25	4	6	**2**

The rate of heat transfer in the study is taken into account by incorporating the Nusselt number. The Nusselt number increases at the increased Reynolds number and the Joule heating parameter. Increased Nusselt number implies that the heat transfer by convection is greater than the rate of heat transfer by conduction. This implies that a

significant amount of heat is generated internally which enhances the convection heat transfer in the fluid. Further, an increase in the Hartmann number and the unsteadiness parameter leads to the decrease in the Nusselt number. This implies that the rate of heat transfer by convection is minimal, while a high rate of heat transfer by conduction is experienced. This shows that a lot of heat is lost into the atmosphere through the conduit's walls by conduction.

5. Conclusion

In this paper, an unsteady, incompressible hydromagnetic flow through a convergent conduit in the presence of variable magnetic field was investigated. The results showed that velocity, temperature, and magnetic induction profiles are high at the centreline which is due to minimal viscosity. Further, the fluid temperature is observed to increase with the increased Reynolds number, Hartmann number, Eckert's number, and Joule heating parameter. On the other hand, the fluid velocity and magnetic induction increase with increase in the Reynolds number, the Eckert number and the Joule heating parameter.

This has remarkable applications in the Pelton turbines, where the end of a pipe is fitted with a convergent nozzle to increase the velocity of the moving water since the Pelton wheel extracts energy from the impulse of the moving water. Therefore, to maintain a high fluid velocity in the conduit, a less viscous fluid should be considered. Similarly, the heat loss at the conduit's wall can be minimized by using appropriate insulators at the wall. This will maximize the rate of heat transfer by convection which consequently increases the fluid velocity. Further, facilitating the Joule heating process by increasing the amount of electric current passing through the conducting fluid will minimize the skin friction coefficient hence increasing the fluid's velocity. The induced magnetic field decreases with an increase in time (unsteadiness parameter). This implies that as time elapses, the reduction of the magnetic field would relatively minimize the retardation of fluid flow due to the Lorentz force.

Further research can be done on hydromagnetic non-Newtonian fluid flow in a convergent conduit taking into account the fluid's chemical reaction, varying pressure gradient, turbulence, and backflow near the conduit's wall.

Data Availability

The data used to support the findings of this study are included within the article.

Conflicts of Interest

The authors declare that there are no conflicts of interest.

Acknowledgments

The authors would like to thank the Jomo Kenyatta University of Agriculture and Technology for support in this project.

References

[1] G. B. Jeffery, "On the steady rotation of a solid of revolution in a viscous fluid," *Proceedings of the London Mathematical Society*, vol. 2, pp. 327–338, 1915.

[2] G. Hamel, "Spiral movements of viscous liquids," *Jahresbericht der Deutschen Mathematiker-Vereinigung*, vol. 25, pp. 34–60, 1917.

[3] L. Ali, B. Ali, X. Liu, T. Iqbal, R. M. Zulqarnain, and J. Muhammad, "A comparative study of unsteady MHD Falkner-Skan wedge flow for non-Newtonian nanofluids considering thermal radiation and activation energy," *Chinese Journal of Physics*, vol. 77, pp. 1625–1638, 2022.

[4] I. S. Nima, S. O. Ferdows, M. Shamshuddin, M. D. Alsenafi, A. Abdulaziz, and A. Nakayama, "Melting effect on non-Newtonian fluid flow in gyrotactic microorganism saturated non-Darcy porous media with variable fluid properties," *Applied Nanoscience*, vol. 10, no. 10, pp. 3911–3924, 2020.

[5] G. R. Rajput, M. D. Shamshuddin, Salawu, and O. Sulyman, "Thermosolutal convective non-Newtonian radiative Casson fluid transport over a vertical plate propagated by Arrhenius kinetics with heat source/sink," *Heat Transfer*, vol. 50, no. 3, pp. 2829–2848, 2021.

[6] J. Nagler, "Jeffery-Hamel flow of non-Newtonian fluid with nonlinear viscosity and wall friction," *Applied Mathematics and Mechanics*, vol. 38, no. 6, pp. 815–830, 2017.

[7] V. Ojiambo, M. Kinyanjui, and M. Kimathi, *A Study of Two-Phase Jeffery Hamel Flow in a Geothermal Pipe*, IJAAMM, 2018.

[8] F. O. Ochieng, M. N. Kinyanjui, and M. Kimathi, *Hydromagnetic Jeffery-Hamel Unsteady Flow of a Dissipative Non-Newtonian Fluid with Nonlinear Viscosity and Skin Friction, [Ph.D. thesis]*, JKUAT-PAUSTI, 2018.

[9] A. T. Akinshilo, A. Ilegbusi, H. M. Ali, and A. J. Surajo, "Heat transfer analysis of nanofluid flow with porous medium through Jeffery Hamel diverging/converging channel," *Journal of Applied and Computational Mechanics*, vol. 3, no. 6, pp. 433–444, 2020.

[10] A. C. Das, N. Q. Novera, Tansue, and M. D. A. Sarwar, "Analysis of magnetohydrodynamic Jeffery-Hamel flow in a convergent-divergent channel using Cu-water nanofluid," *Science*, vol. 12, no. 2, pp. 79–92, 2021.

[11] A. Liagat, A. Bagh, L. Xiaomin, A. Shehzad, and S. Murad Ali, "Analysis of bio-convective MHD Blasius and Sakiadis flow with Cattaneo-Christov heat flux model and chemical reaction," *Chinese Journal of Physics*, vol. 77, pp. 1963–1975, 2022.

[12] M. Faraday, "On the forms and states assumed by fluids in contact with vibrating elastic surfaces," *Philosophical Transactions. Royal Society of London*, vol. 121, pp. 815–830, 1831.

[13] F. W. Sear, "Faraday's law and Ampere's law," *American Journal of Physics*, vol. 6, no. 31, pp. 439–443, 1963.

[14] E. R. Onyango, M. Kinyanjui, and S. M. Uppal, "Unsteady Jeffrey-Hamel flow in the presence of oblique magnetic field with suction and injection," *Applied and Computational Mathematics*, vol. 9, no. 1, pp. 1–13, 2020.

[15] A. Salih, *Conservation Equations of Fluid Dynamics*, Department of Aerospace Engineering Indian Institute of Space Science and Technology, Thiruvananthapuram, 2011.

[16] M. D. Alam and M. A. H. Khan, "Critical behaviour of the MHD flow in convergent-divergent channels," *Journal of Naval Architecture and Marine Engineering*, vol. 7, no. 2, pp. 83–93, 2011.

[17] M. Rahman, *New Approach to Partial Differential Approximants, [M.S. thesis]*, Department of Mathematics, BUET, 2004.

[18] L. F. Shampine, J. Kierzenka, and M. W. Reichelt, "Solving boundary value problems for ordinary differential equations in MATLAB with n4c," *Tutorial Notes*, vol. 2000, pp. 1–27, 2000.